



## Emerging screening platform characterises aminoquinoline structure–activity relationships with phospholipid layers

Bethany Crow<sup>a</sup>, Roland Grafstrom<sup>b</sup>, Vesa Hongisto<sup>b</sup>, Mitali Kamat<sup>a</sup>, Nikil Kapur<sup>a</sup>, Ross Kelly<sup>c</sup>, Josh Owen<sup>a</sup>, Ashi Rashid<sup>a</sup>, William Stokes<sup>a</sup>, Nicola William<sup>a</sup>, Jeanine Williams<sup>a</sup>, Andrew Nelson<sup>a,\*</sup>

<sup>a</sup> Schools of Chemistry and Mechanical Engineering, University of Leeds, Leeds LS2 9JT UK

<sup>b</sup> Misvik Biology Oy, Karjakatu 35 20520 Turku, Finland

<sup>c</sup> Astra Zeneca, UG22 Redesmere, Macclesfield, Cheshire SK10 2NA UK

### ARTICLE INFO

#### Keywords:

Artificial membrane screening platforms  
Aminoquinolines  
Structure–activity  
Biomembrane affinity  
Molecular modelling  
*In-vitro* ToxScore

### ABSTRACT

Aminoquinolines (AQ) and substituted aminoquinolines (s-AQ) interact with electrochemically monitored supported dioleoyl phosphatidylcholine (DOPC) monolayers and immobilised artificial membranes (IAM) on HPLC column. The electrochemical sensor records adsorption/partition of the compound on and into the layer as well as specific interactions due to the location of the compound in the layer. HPLC-IAM technology measures the partition coefficient between the solution and phospholipid including partition due to interaction of the positive molecular charge with the phospholipid polar heads. The monolayer interaction results were combined and normalised for the neutral compounds' lipophilicity as a log biomembrane affinity index ('log BAI') to exemplify charge and structural features in the interaction. A ChimeraX molecular modelling procedure was used to aid in the results interpretation. A compound ToxScore value was derived from 5 *in vitro* assays. The 'log BAI' exhibited a linear relationship with the AQ pK<sub>a</sub> values showing that the interaction was related to the molecular positive charge and to the electron donating properties of the –NH<sub>2</sub> group. The correlation outliers showed a tendency/no tendency to H-bonding with the polar groups and a superficial/deeper location respectively in the phospholipid layer. The s-AQ 'log BAI' value displayed a power correlation with the compounds' ToxScore values.

### 1. Introduction

Structure–activity relationships (SARs) identify those specific properties of a pharmaceutical which are responsible for a particular biological action through analysing the relationship between the compound's structure and that of the target [1]. In this way medicinal chemists can optimise the structure of the drug to enhance its interaction with the target and to prevent adverse effects occurring within the body

[2]. Techniques have thus been developed to predict the efficiency and toxicity of pharmaceuticals, relating their biological outcome to the properties of the compound [3]. An artificial (bio)membrane screening platform has been developed using rapid cyclic voltammetry (RCV), which measures the interaction of a biologically active compound at a given concentration with a phospholipid, dioleoyl phosphatidylcholine (DOPC) monolayer via an electrochemical output of monolayer capacitance change [4,5]. This screening [4] has been carried out together

**Abbreviations:** s-AQ, substituted aminoquinoline; 2-AQ, 2-aminoquinoline; 3-AQ, 3-aminoquinoline; 4-AQ, 4-aminoquinoline; 5-AQ, 5-aminoquinoline; 6-AQ, 6-aminoquinoline; 7-AQ, 7-aminoquinoline; 8-AQ, 8-aminoquinoline; 5-A-6-MeQ, 5-amino-6-methylquinoline; 2-AQ-3-CN, 2-aminoquinoline-3-cyanonitrile; BEAS-2B, human normal bronchial epithelial cells; CHI, chromatographic hydrophobicity index; CTG, CellTiter-Glo; DAPI, 4',6'-diamidino-2-phenylindole; DMSO, dimethylsulfoxide; DNA, deoxyribonucleic acid; DOPC, dioleoyl phosphatidylcholine; DPPC, dipalmitoyl phosphatidylcholine DSB, double-strand break; FPGA, a field-programmable gate array; H2AX, histone protein encoded by H2AFX gene; HPLC, high performance liquid chromatography; IAM, immobilised artificial membranes; LE, lowest energy conformation; LoD, limit of detection; 'log BAI', log biomembrane affinity index; log *D*, log octanol–water distribution coefficient as a function of pH; log *P*, log octanol–water partition coefficient; MIE, molecular initiating event; 8-OHG, 8-hydroxydeoxyguanosine; MP, most probable conformation; PBS, phosphate buffered saline; PQ, primaquine; Q, quinoline; RCV, rapid cyclic voltammetry; SAR, structure–activity relationship; Sit, sitamaquine.

\* Corresponding author.

**E-mail addresses:** [roland.grafstrom@ki.se](mailto:roland.grafstrom@ki.se) (R. Grafstrom), [n.kapur@leeds.ac.uk](mailto:n.kapur@leeds.ac.uk) (N. Kapur), [j.j.owen@leeds.ac.uk](mailto:j.j.owen@leeds.ac.uk) (J. Owen), [a.rashid2@leeds.ac.uk](mailto:a.rashid2@leeds.ac.uk) (A. Rashid), [willstokes@btinternet.com](mailto:willstokes@btinternet.com) (W. Stokes), [nicola.william1@nhs.net](mailto:nicola.william1@nhs.net) (N. William), [j.williams4@leeds.ac.uk](mailto:j.williams4@leeds.ac.uk) (J. Williams), [a.l.nelson@leeds.ac.uk](mailto:a.l.nelson@leeds.ac.uk) (A. Nelson).

<https://doi.org/10.1016/j.bioelechem.2025.108927>

Received 13 November 2024; Received in revised form 28 January 2025; Accepted 31 January 2025

Available online 1 February 2025

1567-5394/© 2025 The Authors. Published by Elsevier B.V. This is an open access article under the CC BY license (<http://creativecommons.org/licenses/by/4.0/>).

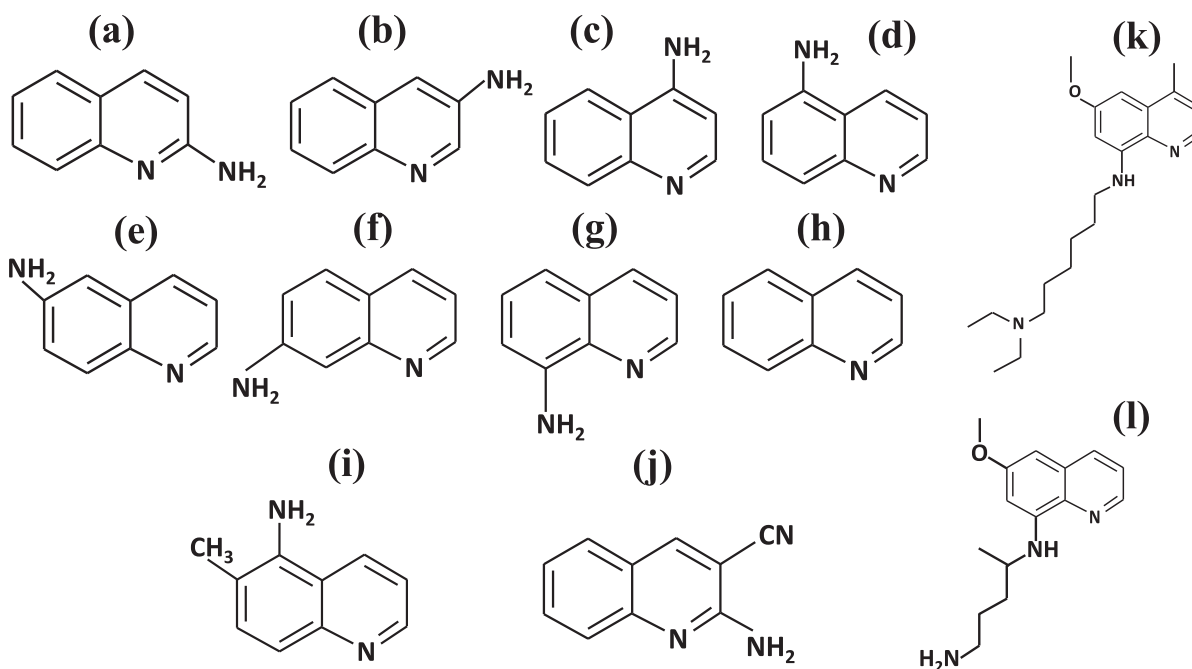


**Fig. 1.** Structures of AQ and *s*-AQ molecules studied: (a-g) 2 to 8-AQ, (h) Q, (i) 5-A-6-MeQ, (j) 2-AQ-3-CN, (k) PQ and (l) Sit.

with three other established technologies to broaden the investigation and to validate the electrochemical approach. These technologies included, immobilised artificial membrane chromatography (IAM), molecular modelling and *in vitro* screens. However although IAM measures the partition of the compounds into the phospholipid phase, the previous study (4) showed that the electrochemical membrane sensor's output was related to additional characteristics of the compounds above that of molecular partition. The present study was carried out to further develop this integrated screening platform and to establish exactly which structural features of the molecule are responsible for their interaction with the phospholipid layers and the biological relevance thereof.

Quinolines were chosen as an effective set of demonstrator compounds for the current work. These compounds provide the scaffold to a significant number of the necessary antimalarial medicines [6], such as primaquine [6], amodiaquine [7] and chloroquine [8] as indicated by the World Health Organisation [9]. Although these drugs have been at the forefront of treating malaria; in recent years, there has been a dramatic increase in the malaria parasite's resistance to quinoline-based compounds due to mutations in the parasite's structure [10,11]. This has led to the further development of quinolines for regions of the world that house such drug-resistant parasite strains associated with an increased understanding in the way these pharmaceuticals work. A possible simple structural modification of the compounds would be the adjustment of the amino group situated on the quinoline ring system. For example, most quinoline based malaria drugs [12] consist of the amino group being positioned at the 4th or 8th carbon on the quinoline ring (Fig. 1). No reason has been given for favouring the 4- and 8-aminoquinoline over the other amino positions. Quinolines bypass multiple membranes to reach the parasitic target locations: either at the early stages of malaria, in the liver, or at the later stage, in the red blood cells [12]. Indeed the interaction of primaquine and sitamaquine with cell cultures has been studied and a biomembrane interaction mechanism with both of these compounds has been hypothesised [6,13]. By combining the mechanistic knowledge and the interest in the structural changes of quinolines and their (bio)membrane interaction, it was proposed that such compounds would interact with the phospholipid sensor layer of the screening platform. It was interesting also to discover

why other amino positions on a quinoline skeleton were not used for treatments. This led to this study being initiated with the ultimate aim of determining a SAR between the quinolines and their derivatives, and their activity on the phospholipid layer.

The compounds selected for this project were a group of quinolines, including marketed pharmaceuticals, ranging in functional groups and their positioning. The study was carried out in a systematic manner looking at: (a) quinoline (Q) as a control compound, (b) the aminoquinolines (AQ) with the amino group at positions 2 to 8, (c) two substituted aminoquinolines (*s*-AQ) with the methyl and cyano groups as substituents respectively, 5-A-6-MeQ and 2-AQ-3-CN and, (d) two *s*-AQ with alkyl chains terminating in an ionisable amino group ie primaquine (PQ) and sitamaquine (Sit) respectively (see Fig. 1). These compounds were chosen so that the effect of the (i) amino group position and (ii) the nature of the substituent, on the interaction of the Q and AQ respectively with a phospholipid layer could be ascertained. Intuitively the interaction of AQ and *s*-AQ with phospholipid layers and the relation of their structure thereto presents an insightful problem. Generally there are four properties of small organic molecules which determine their affinity towards phospholipid layers which include, lipophilicity [14], charge [15], H-bonding propensity [16] and polarisability [17]. Both the lipophilicity and the molecular charge are non-specific properties of the molecule characterised by their log *P* value and charge number respectively. The log *P* value can be corrected for charge to log *D* at a given solution pH for ionisable molecules assuming the ionised molecule is not lipophilic [18]. Both the H-bonding propensity and polarisability are molecular and electronic properties which influence the specific non-covalent binding of a molecule to the polar groups and the alkyl chains respectively of a phospholipid layer. The AQ and *s*-AQ represent an ideal "test-bed" for relating their respective structures and properties to their interactions with phospholipid layers. For the AQ, the compound's pK<sub>a</sub> is directly associated with the position of the amino group and the delocalisation of the amino group's lone pair electrons with the Q ring structure. This electron donating property of the amino group derived from its Hammetts constant will determine the polarisability of the Q rings [19]. In addition the lipophilicity of a given aqueous concentration of given pH (log *D*) of AQ depends not only on its log *P* value but also on its pK<sub>a</sub> assuming only the neutrally charged molecule is

**Table 1**

AQs and s-AQs: solution properties where  $\log D_{(\text{pH}=7.4)} = \log P - \log[1 + 10^{(\text{pK}_a - 7.4)}]$  [18]. Superscript *p* denotes predicted average as opposed to experimental value.

Compound	pK <sub>a</sub>	log <i>P</i>	log <i>D</i> <sub>(pH=7.4)</sub>
2-AQ	7.34 [21]	1.87 [22]	1.60
3-AQ	4.95 [21]	1.63 [22]	1.63
4-AQ	9.17 [21]	1.63 [22]	-0.15
5-AQ	5.46 [21]	1.16 [22]	1.16
6-AQ	5.63 [21]	1.28 [22]	1.27
7-AQ	6.65 [21]	1.32 [22]	1.25
8-AQ	3.99 [21]	1.79 [22]	1.79
Q	4.94 [21]	2.03 [22]	2.03
5-A-6-MeQ	7.19 [22 <sup>p</sup> ]	1.68 [22 <sup>p</sup> ]	1.47
2-AQ-3-CN	3.87 [22 <sup>p</sup> ]	1.89 [22 <sup>p</sup> ]	1.89
PQ	9.69 [22 <sup>p</sup> ]	2.79 [22 <sup>p</sup> ]	0.50
Sit	10.6 [22 <sup>p</sup> ]	5.18 [22 <sup>p</sup> ]	1.98

lipophilic [20]. The individual AQ's pK<sub>a</sub> value will also determine its charge at a given pH. All AQs will have a specific orientation in the phospholipid layer related to their amino group position and this orientation will determine the extent of H-bonding between the amino group and the phospholipid polar groups. The s-AQs represent a more complex case in that the lipophilicity and electron donating properties of the substituent will influence the s-AQs' interaction with phospholipid as well as the effect of the substituent on the molecule's pK<sub>a</sub> and overall lipophilicity. Table 1 lists values of log *P*, pK<sub>a</sub> and the derived log *D* values of AQs and s-AQs studied.

The study described in this paper is composed of a several pronged approach with the following objectives:- (1) to validate the electrochemical (bio)membrane sensor as an emerging technology within a composite screening platform on a set of well-chosen small organic molecule demonstrator molecules as described above, and (2) to use the results from the applied technologies to evaluate exactly how the structure of the molecules determines its interaction with phospholipid layers and how this is related to the molecules' interaction with selected biological targets through *in vitro* assays. As detailed above the demonstrator compounds are the AQs and the s-AQs and the technologies used to study their interactions are; (a) Electrochemical (bio) membrane sensor, (b) HPLC with the immobilised artificial membrane (IAM) technology as the reverse phase [23], (c) Use of CHARMM [24], ChimeraX [25] and AUTODOCK 4.2 [26,27] software for estimating the position and H-bonding of AQs and s-AQs in DOPC phospholipid bilayers, and (d) Comprehensive high throughput *in vitro* screens [28] specifically using BEAS-2B cells assayed in the presence and absence of 10 % serum with five different endpoints.

The electrochemical sensor reported in this paper is proposed as an alternative procedure for screening pharmaceutical compounds for putative biomembrane activity and deducing structure–activity relationships therefrom. This technology has previously been compared with *in vitro* assessments of the cytotoxicity of three bioactive compounds [29]. An identical *in vitro* toxicity ranking of the compounds to that of the electrochemical platform was obtained. However the electrochemical procedure took 5 min per compound to carry out whereas the *in vitro* toxicity procedures took more than 3 h to complete excluding the time taken for cell culture preparation. In addition the electrochemical procedure was more than ten times sensitive than the *in vitro* cytotoxicity tests. The most significant pharmaceutical/toxicant screening method which compares with the electrochemical (bio)membrane sensor is the HPLC-IAM technology [4,23]. For this reason we have compared and combined respectively the (bio)membrane sensor results with those from the IAM-HPLC platform. In principle the metrics from the IAM-HPLC procedure record a distribution coefficient (*K*<sub>IAM</sub>) between the mobile phase and the tethered phospholipid reverse phase which is related to the lipophilicity of the interacting compound [4,23] and its positive charge [15]. The procedure is also selective since each compound passing through the HPLC column has a specific retention time.

The electrochemical (bio)membrane sensor records a metric (–log LoD) which is characteristic of the affinity of the compound for the mobile phospholipid layer [4,5]. This metric is related to the lipophilicity and the positive charge of the interacting compound and also to specific molecular aspects of the interaction including H-bonding and non-covalent interactions. However the (bio)membrane sensor response is not selective to a particular compound within a mixture of compounds. Similar to the *in vitro* toxicity test, it records a global response representative of the biomembrane activity of the compound(s) [4,5].

## 2. Materials and methods

### 2.1. Electrochemical (bio)membrane sensor

The twelve compounds of AQs and s-AQs (Fig. 1 and Table 1) were obtained from Sigma-Aldrich. The electrolyte used in the electrochemical experiments was 0.0138 mol/dm<sup>3</sup> NaCl and 0.00027 mol/dm<sup>3</sup> KCl buffered at pH 7.4 with 0.00119 mol/dm<sup>3</sup> phosphate in 18.2 M.Ω cm Milli-Q water (hereinafter in the text referred to as PBS). The PBS was of analytical grade and purchased from Sigma-Aldrich. The compounds were dissolved in methanol to form multiple stock concentrations and further diluted in PBS. Multiple working solutions, with methanol < 2 %, were prepared to ensure the compounds interacted with the (bio)membrane sensor element to give a calibration curve. The microfabricated platinum electrodes (Hg/Pt) used in the electrochemical assay [30,31] were supplied by the Tyndall National Institute, Ireland. The dioleoyl phosphatidylcholine (DOPC) was obtained from Avanti Polar Lipids Alabaster, AL, USA and was > 99 % pure. The DOPC dispersion for electrode coating was prepared by gently shaking DOPC with PBS to give a 0.25 μmole/cm<sup>3</sup> dispersion. All other chemicals and reagents were of analytical grade and purchased from Sigma-Aldrich.

For the assay, the fabricated Hg/Pt electrode was contained in a high-throughput screening platform consisting of a microfluidic flow cell containing the DOPC monolayer supported on the Hg/Pt electrode, four automated bespoke syringe pumps enabling storage and transportation of fluids (electrolyte, test sample, DOPC and water) into the flow cell, a field-programmable gate array (FPGA) data acquisition, and a control unit used to interface between software and hardware and an ACM Research Potentiostat for electrochemical measurements. A laptop was connected to control the screening platform, interfacing with syringe pumps and the FPGA control unit. The microfabricated electrode was prepared in advance by cleaning in a 1 mol/dm<sup>3</sup> solution of NaOH in methanol, followed by HCl and Milli-Q water and then dried. Hg was manually deposited on the Pt disc of radius 0.480 mm to give a Hg/Pt electrode. The electrode was mounted as specified in Owen et al. [30]. Subsequently, all samples of AQ/s-AQ solution, DOPC, electrolyte were deoxygenated with argon gas (Air Products) for a minimum of 30 min. Once purged, three syringes were filled with AQ/s-AQ sample solution (5 mL), DOPC dispersion (60 mL) and PBS (60 mL), respectively, and connected to tubing. Before any analysis, all tubing was flushed with deoxygenated PBS, and any bubbles were removed from the cell. Turning the potentiostat to run, the system was set to:- (i) clean electrode with the electrochemical rejection of the previous used monolayer, (ii) deposit DOPC from dispersion, (iii) test the monolayer integrity in PBS and (iv) screen the sample solution as described previously in refs [30,31] and in Table S1 in the SI. Upon single-sample completion, the sample tubing was flushed with PBS (5 mL). This was the analytical cycle for each sample. Samples were measured at increasing concentrations of one AQ/s-AQ sample, then switching to the next AQ/s-AQ sample. The sample syringe was replaced with every repeat of the same sample and between AQ/s-AQ sample solutions. All measurements were carried out in triplicate, and five or more AQ/s-AQ concentrations were screened for each specific compound All fits to the data were carried out using the program IGOR Pro 9.

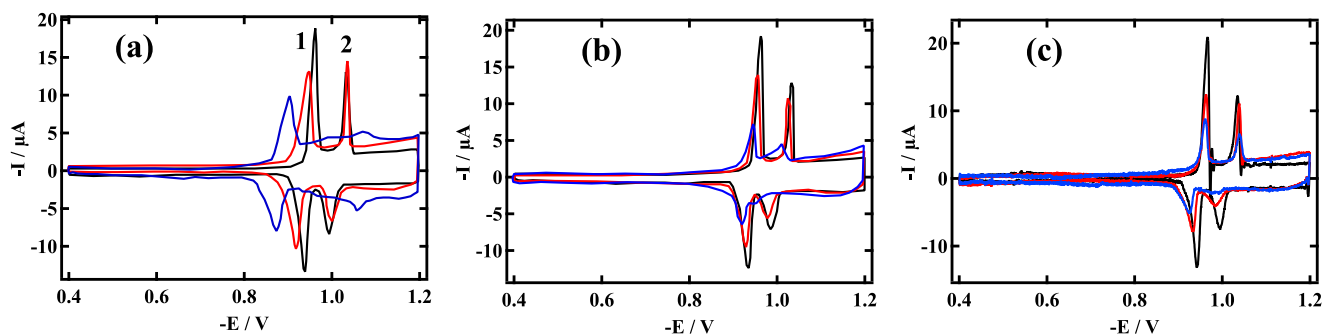


Fig. 2. Representative RCVs of AQ solution concentrations of, (a) 2-AQ, red 1 and blue 10  $\mu\text{mole}/\text{cm}^3$  (1 and 2 refer to capacitance current peaks 1 and 2); (b) 5-AQ, red 1 and blue 2 and (c) 7-AQ, red 0.01 and blue 0.1  $\mu\text{mole}/\text{cm}^3$  interactions with DOPC monolayer. Vertical scale adjusted to control peak height.

## 2.2. HPLC-IAM

Materials used were AQ and *s*-AQ compounds, dimethylsulfoxide (DMSO), HPLC grade ammonium acetate, ( $\text{NH}_4\text{CH}_3\text{CO}_2$ ), NaOH and acetonitrile. AQ and *s*-AQ compounds were added to separate 10 mL vials and diluted with 10 mL DMSO to produce 10  $\text{mmol}/\text{dm}^3$  stock solutions. Assays were carried out in triplicate. Serial dilutions of stock solutions in DMSO were prepared to give 1 and 0.1  $\text{mmol}/\text{dm}^3$  samples in separate 2 mL HPLC vials. Samples were screened on an Agilent 1260 Infinity II HPLC with Diode Array Detector, using a Regis Technologies IAM.PC.DD2, 4.6 mm x 100 mm, 10  $\mu\text{m}$ , column. The mobile phase consisted of a gradient method starting at 100 % pH 7.4 aqueous phase of 0.05  $\text{mol}/\text{dm}^3$   $\text{NH}_4\text{CH}_3\text{CO}_2$ , + NaOH to 10 % with 90 % acetonitrile at 4.75 min; kept constant at 90 % acetonitrile to 5.25 min; then re-equilibrated to 100 % aqueous phase from 5.25 to 5.5 min. An injection volume of 5  $\mu\text{L}$  was used with a flow rate of 1.5 mL/min, and a detection wavelength of 250 nm. The retention time of each compound was determined and converted to the chromatographic hydrophobicity index ( $\text{CHI}_{\text{IAM}}$ ) using the equation of the calibration plot of  $\text{CHI}_{\text{IAM}}$  against retention times (see Fig. S1 in the SI.). Once the  $\text{CHI}_{\text{IAM}}$  values are obtained, they were converted, using the following equations into  $\log k_{\text{IAM}}$  and  $\log K_{\text{IAM}}$  parameters (32).

$$\log k_{\text{IAM}} = (0.046 \times \text{CHI}_{\text{IAM}}) + 0.42 \quad (1)$$

$$\log K_{\text{IAM}} = (0.29 \times e^{\log k_{\text{IAM}}}) + 0.7 \quad (2)$$

## 2.3. ToxScore in vitro assays

High throughput screens using BEAS-2B cells were assayed in the presence and absence of 10 % Foetal Bovine Serum with 0-, 6-, 24- and 72-hour exposure timepoints. The AQs and *s*-AQs were first dispersed in either methanol or DMSO as appropriate. The compounds were further diluted and the assays carried out in LHC-9 cell culture medium from Gibco/Thermo-fisher [32–36]. The pH of this cell culture medium is reported to be 7.3. Five endpoints were employed: (a) CellTiter-Glo (CTG) cell viability assay, (b) DAPI where a nuclear and chromosome counterstain, DAPI (4',6-diamidino-2-phenylindole) emits blue fluorescence upon binding to AT regions of DNA, (c) Caspase 3/7 which identifies apoptotic cells, (d) 8OHG which identifies nucleic acid oxidative stress damage and, (e) H2AX histone phosphorylation which represents an early event in the cellular response against DNA double-strand breaks (DSBs). Screens were carried out in four biological replicates and eight concentrations for each compound were used. The calculation of ToxScore therefrom is described in detail in the SI. No error bars are displayed in the diagrams since the ToxScore is a global measurement combining data from five different endpoints and timepoints and the endpoints are not designed to be as much alike as possible but to represent different toxicity readouts. The most important outcome of the ToxScore measurement is the ToxScore number and the way in

which this compares with the output of the electrochemical (bio)membrane sensor and the IAM-HPLC.

## 2.4. Computational modelling of interaction of AQ and *s*-AQ molecules with the DOPC bilayer

The DOPC bilayer was generated using web software “CHARMM-GUI” [24] in the form of a PDB file. AQ and *s*-AQ structures were modelled and pre-prepared for docking using software “AVOGADRO” and PDB files were generated. Docking of DOPC bilayer and AQ and *s*-AQ was carried out using software “AUTODOCK 4.2” [26,27]. This was done by setting 100 output docked conformations for each compound with the DOPC bilayer. For each AQ and *s*-AQ, lowest energy (LE) docked conformation and conformation with lowest energy with highest number of conformers formed (MP) were selected from the cluster for visualisation of interaction of these compounds with the DOPC bilayer. “ChimeraX” [25] was used for the visualisation of interaction of LE and MP conformers with DOPC bilayer due to non-covalent interactions such as H-bond, halogen bond, aromatic hydrogen bond, salt bridges and  $\pi$  interactions such as  $\pi$ - $\pi$  stacking and  $\pi$ -cation bonding.

## 3. Results and discussion

The system of a phospholipid monolayer adsorbed on a Hg electrode as a biomembrane model has

been developed over four decades [37–39]. It has had fundamental biophysical applications for example in analysing ion channel [40], co-enzyme activity [41] and phospholipid behaviour in electric field [42–44]; however, its predominant practical implementation has been used in modelling the biomembrane activities of molecular [4,5,45] and nanoparticle species [45,46]. Originally, a modified Langmuir–Blodgett technique was used for depositing the phospholipids on to a hanging mercury drop electrode [38,39]. Since these techniques were inappropriate for rapid and routine screening, the electrode was reconfigured as a microfabricated Hg on Pt film electrode [30,31,47], and the phospholipid deposition was enabled from vesicles in a flow cell [30,31]. In this study, a DOPC monolayer is deposited on the Hg electrode on the prepared Pt support and scanned at 40 V/s from  $-0.4$  to  $-1.2$  V referred to throughout the text as rapid cyclic voltammetry (RCV) [30,31,47] (see Table S1 in the SI for full details of screening program). An unsaturated lipid DOPC is chosen for these experiments since it is fluid at room temperature and mobile. For this reason it forms stable monolayers with no defects or boundary lines since it is entirely physically compatible with the supporting liquid mercury surface [39]. Accordingly, the potential induced phase transitions are sharp and very reproducible and their alteration in shape and position is very sensitive to the layer structure and layer interaction with solution compound [4]. DPPC does not form such stable monolayers on mercury and although it exhibits analogous potential-induced phase transitions, these are not as

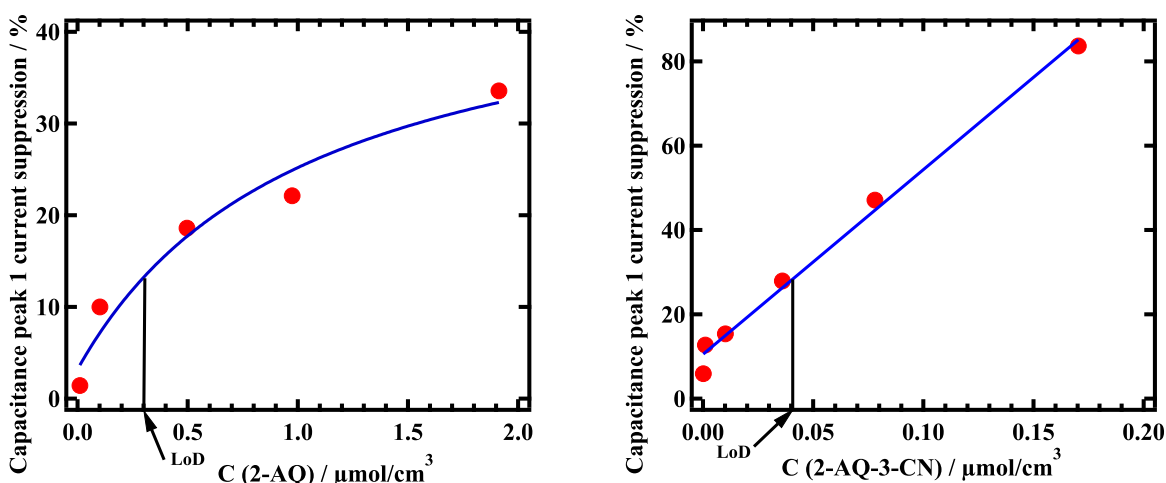


Fig. 3. Representative plots of RCV capacitance peak suppression vs AQ and (b) *s*-AQ concentration. Vertical line normal to horizontal axis denotes LoD thereon.

sharp as those from DOPC [38]. Qualitatively egg-PC which is a mixture of unsaturated and saturated lipids shows a similar interaction with polycyclic aromatic compounds as DOPC [observed but not published]. Finally DOPC mirrors the fluidity of cell membranes [48] and therefore is a more biologically relevant sensor layer to relate to the biomembrane activity of the interactive compounds.

The most effective and sensitive capacitance-based phospholipid layer sensor only functions with Hg as the conductive support. The infinitely smooth surface of liquid Hg is physically compatible with the fluid DOPC phospholipid layer. This enables a stable, mobile phospholipid layer to remain on the Hg support. The DOPC layers on Hg undergo potential-induced phase transitions characterised by two sharp capacitance current peaks (voltammetric), 1 and 2, respectively, as shown in Fig. 2 [30,31,47]. These two peaks correspond to the penetration of electrolyte into the layer and the reorganisation of the monolayer to form bilayer patches, respectively [42–44]. Only on Hg are the capacitance current–potential curves obtained which are entirely reproducible over multiple scans and consist of sharp reproducible discontinuities coincident with potential-induced phase transitions. In contrast phospholipid bilayers on solid electrodes do not exhibit these sharp capacitance peaks coincident with potential-induced phase transitions [49]. In addition, solid supported bilayers are often tethered to the electrode [50,51] and this by definition renders at least one layer of the bilayer immobile in contrast to the free floating monolayers on Hg. The technology using fabricated Hg/Pt electrodes has been developed to render the platform more easy to handle and environmentally acceptable. The Hg (~1 mg) is deposited on Pt microelectrodes on fabricated wafer. The Hg bonds to the Pt and the wafer is sealed within a flow cell. This fabricated electrode can be used within the flow cell for up to several months through many screenings. Lipid deposition and electrode cleaning are carried out automatically throughout the whole screening cycle (5 min). The technical operator need never open the flow cell between screenings and thus never comes into contact with Hg.

Changes in the capacitance peaks represent changes in the structure of the monolayer [30,31,47]. The interaction of the test substance with the monolayer selectively and systematically influences the capacitance-current potential profile [4,5,45,46]. An interaction of the test substance with the polar groups of the DOPC is reflected in a depression of the two peaks [4,5,45,46] while an increase in the baseline of the capacitance current reflects the association of a polar compound with the apolar region of the DOPC layer and/or its disruption [4,5,45,46]. The reason for the latter effect is that the low value of baseline capacitance current is representative of the ordered DOPC layers on the electrode with the low dielectric apolar lipid tails adjacent to the electrode surface. When this low dielectric region is penetrated by a higher dielectric compound,

the average dielectric constant of this region increases leading to an increase in the baseline capacitance current [4,5,45,46]. A potential shift in the capacitance current peaks indicates a change in the potential profile across the layer caused by the interaction of the compound with the layer [4,52]. A monolayer disordering is shown as a broadening of the peaks [4,45]. The screening results from this sensor platform have recently been shown to be related to biomembrane damage in *in vitro* cell cultures [29]. Other research groups have followed a similar approach, but not in rapid *online* screening format [53–55].

Fig. 2 and more comprehensively Fig. S2 in the SI display RCVs from the interactions of AQ and *s*-AQ compounds with the DOPC. The effect of the interaction on the RCV profile is to suppress the height of the capacity current peaks. Interestingly the influence of 2-,3- and 4-AQ interaction with the DOPC layer on the RCV is to shift capacitance current peak 1 to significantly more positive potentials with increase in solution AQ concentration. However, the effect of 5- and 6-AQ interaction with the DOPC layer on the RCV is to induce less of a positive potential shift to the capacitance peak 1 current and the effect of 7- and 8-AQ interaction with the DOPC layer on the RCV is to induce no significant potential shift to the capacitance peak current. The same lack of capacitance current peak shift is observed when Q and the *s*-AQs interact with the DOPC layer (Fig. S2 in the SI).

Generally when the suppression of the capacitance current peak 1 is plotted against the solution concentration (see Fig. 3 and Fig. S3 in the SI) a curvilinear response is observed which can be fitted to the Langmuir equation implying that the DOPC layer is becoming in part saturated with the compound at higher solution concentrations expressed as [56]:-

$$Y = a + [bX/(100 + cX)] \quad (3)$$

For a few interactions the extent of capacitance peak 1 depression with respect to solution concentration is linear. In this case the calibration curve is fitted to a linear equation [56]:-

$$Y = a + cX \quad (4)$$

Where Y is the % current peak depression, X is the solution concentration of AQ or *s*-AQ, 'a' is the intercept due to some depression of the control current peak during the assay. Since the most significant metric in this study is the compound interaction at low concentration as the molecular initiating event (MIE), the shape of the calibration curves and the reasons therefor will not be investigated further in this study. The LoD metric of the AQ and *s*-AQ affinity for the DOPC monolayer is the lowest significant solution concentration of compound which can structurally modify the DOPC layer and is estimated from three times the

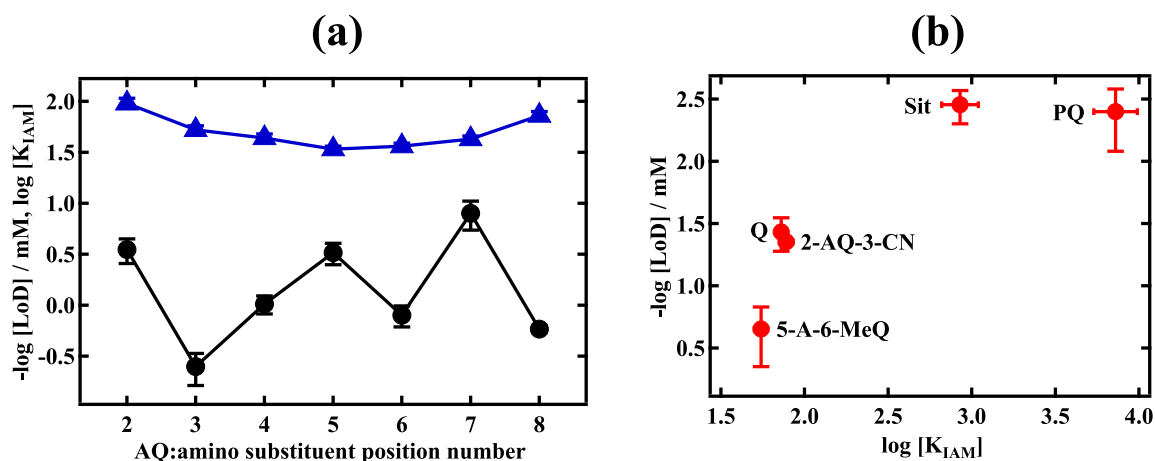


Fig. 4. Plots of: (a)  $-\log \text{LoD}$  (black circle) and  $\log K_{\text{IAM}}$  (blue triangle) versus the amino position number on AQ and (b)  $-\log \text{LoD}$  versus the  $\log K_{\text{IAM}}$  for s-AQ/phospholipid interaction.

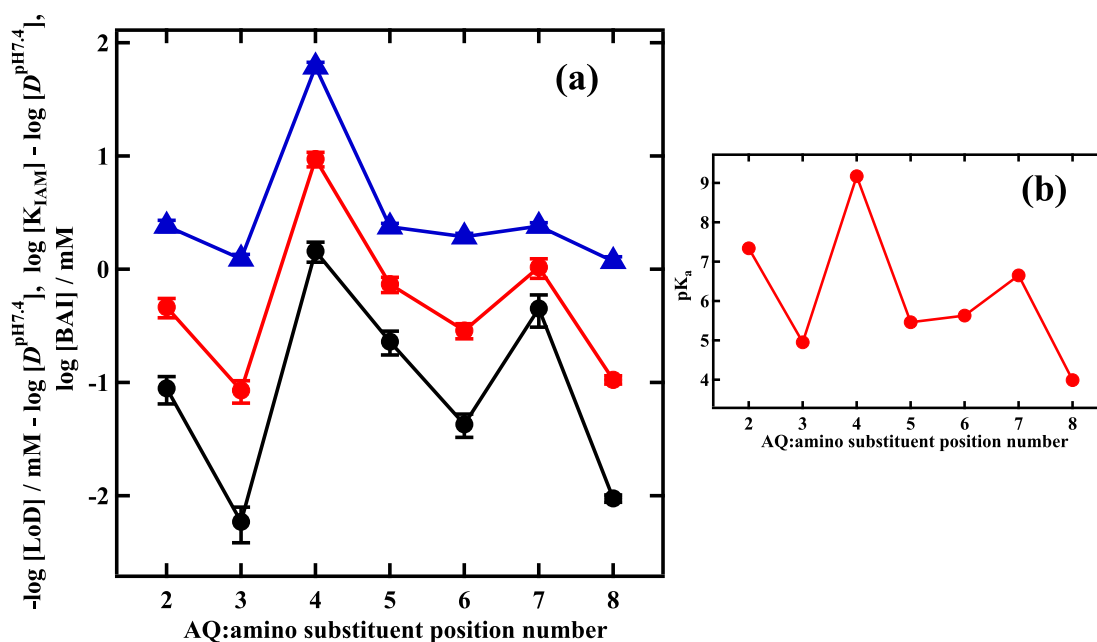


Fig. 5. (a)  $-\log \text{LoD} - \log D$  (black circle), 'log BAI' (red square),  $\log K_{\text{LW}} - \log D$  (blue triangle) and (b)  $\text{pK}_a$  of the AQs versus the amino substituent position number.

standard deviation of the DOPC capacitance peak 1 current corresponding to the AQ and s-AQ solution concentration on the appropriate calibration curve [4,5]. The LoD error is taken from the error of the slope coefficient for the linear plot and the mean of the errors associated with both coefficients for the Langmuir plots, respectively. The LoD metric was expressed as  $-\log \text{LoD}$ . Both  $-\log \text{LoD}$  and  $\log K_{\text{IAM}}$  include lipophilic and other monolayer affinity parameters due to the molecules' H-bonding propensity, polarisability and charge. This study has therefore "normalised" both the  $-\log \text{LoD}$  and  $\log K_{\text{IAM}}$  metrics by subtracting the  $\log D$  value for the compound from each metric. This effectively expresses the two metrics as representing the monolayer affinity of the compounds above that of the lipophilicity of the neutral molecule. The aim here was to extract mechanistic details of the AQ and s-AQ interaction with the lipid layers. Table S2 in the SI lists  $-\log \text{LoD}$  and  $\log K_{\text{IAM}}$  values obtained in this study from compounds displayed in Fig. 1 together with derived values of  $-\log \text{LoD} - \log D$  and  $\log K_{\text{IAM}} - \log D$  values.

Fig. 4(a) and 4(b) displays plots of  $-\log \text{LoD}$  and  $\log K_{\text{IAM}}$  versus the

amino position number of AQ and plots of  $-\log \text{LoD}$  versus  $\log K_{\text{IAM}}$  for s-AQ interaction respectively with phospholipid layers. The difference between the values of  $-\log \text{LoD}$  and  $\log K_{\text{IAM}}$  in these plots reflects that these techniques measure different modes of interaction. The  $-\log \text{LoD}$  represents the interaction between the AQ in the aqueous phase and a highly mobile DOPC layer and the  $\log K_{\text{IAM}}$  represents the partition between the aqueous AQ and a phospholipid layer covalently bound to a silica bead phase respectively. Significantly (Fig. 4(a)) the AQ  $\log K_{\text{IAM}}$  displays a slight decrease then increase with amino position number whereas the  $-\log \text{LoD}$  displays three maxima corresponding to 2-, 5- and 7-AQ. Furthermore for the s-AQ/phospholipid interaction, the slope of  $-\log \text{LoD}$  versus  $\log K_{\text{IAM}}$  is steep at low  $K_{\text{IAM}}$  values but levels off at higher  $\log K_{\text{IAM}}$  values (see Fig. 4(b)). The curvilinear relationship between the two parameters is evident and also reflects the difference between the methodologies and the sensor layer configuration. Whereas the  $\log K_{\text{IAM}}$  reports on a phase distribution between aqueous solution and phospholipid layer of unlimited area within a chromatographic column, the  $-\log \text{LoD}$  metric measures the same including specific

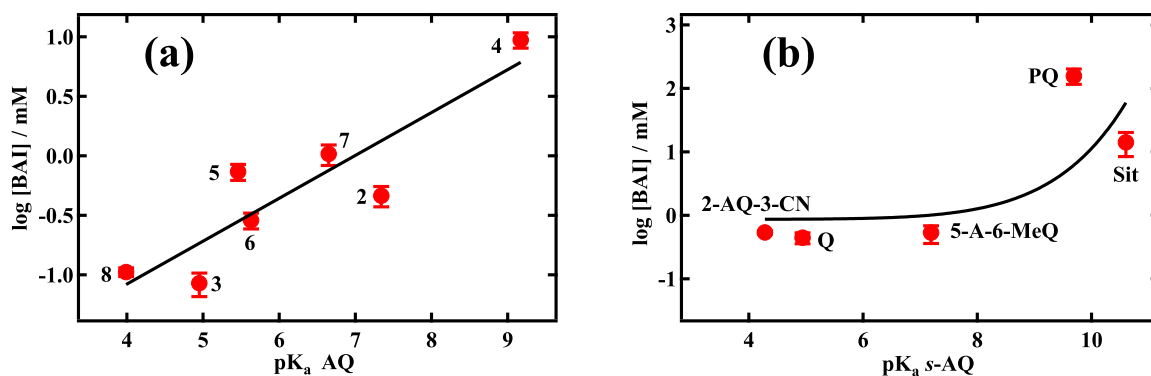


Fig. 6. Plots of 'log BAI' of (a) AQ and (b) s-AQs vs their  $pK_a$  value.

interactions with a fluid DOPC layer on a limited coated electrode surface area.

Fig. 5(a) displays plots of  $-\log \text{LoD} - \log D$  and  $\log K_{\text{IAM}} - \log D$  of the AQs versus the amino position number. On subtracting  $\log D$  from  $\log K_{\text{IAM}}$  and  $-\log \text{LoD}$  the vertical axis values peak when the amino group is at the 4- and 2-, 4- and 7- positions respectively. If we assume that both values are representative of membrane affinity above that due to the lipophilicity of the neutral molecule with associated experimental bias as well as the effect of the silica column material in IAM [57], their mean value defined as  $(-\log \text{LoD} + \log K_{\text{IAM}} - 2 \cdot \log D)/2$  will be a more accurate indicator of the compound's affinity above the lipophilicity for a biomembrane-like layer. We therefore term this value as the log biomembrane affinity index ('log BAI'). The physical meaning of 'log BAI' or biomembrane affinity index is that it represents those molecular properties which enhance interaction of a molecule with the biomembrane-like sensor layer over the molecule's general lipophilicity at a defined solution pH as quantified by  $\log D$ . The 'log BAI' includes charge as a non-specific molecular property and it also includes the tendency to form specific interactions of H-bonding between the molecule and the phospholipid polar groups and non-covalent associations between the molecule's aromatic rings/unsaturated substituents and the alkyl chains of the phospholipid. The 'log BAI' approach has been newly developed in this study. In principle it could be used in any membrane sensor application where an interaction is observed between a compound in the aqueous phase and the sensor phospholipid layer. The log of the distribution metric(s) obtained can be normalised by compound  $\log D$  to give a 'log BAI' value. The 'log BAI' value is plotted against the amino group position in Fig. 5(a). A list of derived 'log BAI' values is displayed in Table S2 in the SI. In Fig. 5(b),  $pK_a$  values of the AQs are plotted versus the amino position number and it is observed from Fig. 5 (a) and 5(b) that the 'log BAI' and  $pK_a$  respectively vs amino position number almost directly superimpose on each other except for the 'log BAI' for 5-AQ/phospholipid interaction. The  $pK_a$  is plotted for comparison as compound descriptor to the experimental values in Fig. 5(b) since the  $pK_a$  magnitude relates both (i) to the stability of the protonated AQ due to delocalisation of electrons from the  $-\text{NH}_2$  group on to AQ rings and, (ii) to the extent of positive charge on the AQ at pH 7.4 [58].

Results in Fig. 5(a) and 5(b) can be summarised in Fig. 6(a) which show a correlation between the AQ 'log BAI' and the  $pK_a$  which, as expected, is good except for outliers, 2- and 3- and 5-AQ.

As stated above, the 'log BAI' value is composed of the following factors:- (i) the charge on the compound, (ii) the tendency of the compound to form non-covalent associations with the phospholipid layer due to its polarisability, and (iii) the effect of the amino group position on the orientation of AQ following its insertion into the phospholipid layers. For the AQs only 2-, 4-, 5- and 7-AQ can be depicted tautomatically as imines which allow the electrons from the amino group to be delocalised on to the quinoline rings [58]. Fig. S4 in the SI shows that both 2- and 4-AQ have resonance structures in unprotonated and

protonated forms respectively where the Kekule structure of one of the quinoline rings is preserved. This will lead to some delocalisation of the  $\text{NH}_2^-$  electron pair with the aromatic ring so increasing the electron density of the ring. The high  $pK_a$  value of 4-AQ has already been attributed to the stability of the protonated compound [58]. The lower  $pK_a$  value of 2-AQ can be related to the lower stability of the protonated imine which has a less stable orthoquinonoid structure [58]. For 5- and 7-AQs the Kekule structure of both rings disappears in the AQ resonance structure and the corresponding protonated imine, and the compounds'  $pK_a$  values are respectively lower [58].

From the  $pK_a$  values we can calculate the proportion of charged AQ present in aqueous buffer at pH 7.4 for 4-, 2-, 7- and 5-AQ as 98, 47, 5.4 and 1 % respectively. Since both AQ positive charge and delocalised electrons on the quinoline ring in the neutral molecule promote AQ interaction with the phospholipid layer, we can say that the 'log BAI' peak for 4-AQ interaction is entirely due to the affinity of the protonated 4-AQ for the layer since organic cations have an affinity for zwitterionic phospholipid bilayers and monolayers through interaction with the negatively charged phosphate moieties of the polar groups [6,59–61]. On the other hand for the 2-, 7- and 5-AQ interactions with the layer, the presence of delocalised electrons on the quinoline rings plays a role in the AQs' increased affinity for the layer over its lipophilicity alone. The orientation and location of the AQ in the DOPC layer will also affect its affinity for the layer above the AQ's lipophilicity. As can be seen in Fig. 2 and Fig. S2 in the SI, the RCVs of 2-, 3- and 4-AQ/DOPC interaction show a significant positive potential shift of the capacitance current peaks which is not so significant in the RCVs of 5-, 6-, 7- and 8-AQ/DOPC interaction. This could be identified with a factor which has a systematic influence on the respective AQ's affinity for the DOPC layer.

The 'log BAI' value for 5-A-6-MeQ interaction with the phospholipid layer ( $-0.27$ ) is lower than that estimated for the 5-AQ interaction ( $-0.13$ ) which is due the increased molecular hydrophobicity from the  $\text{CH}_3^-$  group without a corresponding increase in specific binding within the phospholipid layer. This is in spite of the 5-A-6-MeQ being 38 % positively charged at pH 7.4. The RCV for 2-AQ-3-CN shows no shift in capacitance current peak potential in contrast to that which is observed for 2-AQ/DOPC interaction (see Fig. 2). In addition the  $-\text{CN}$  group is strongly electron withdrawing with positive Hammetts constants of 0.61 and 0.66 [62] although the 'log BAI' values for this compound's interaction with the phospholipid layer is higher ( $-0.27$ ) than that of 2-AQ/phospholipid interaction ( $-0.34$ ). In this case it seems that the highly polarisable  $-\text{CN}$  group instigates the interaction with a different orientation of this compound in the phospholipid layer compared to that of 2-AQ. Fig. 6(b) shows the relationship of 'log BAI' values of quinoline (Q), 5-A-6-MeQ, 2-AQ-3-CN, primaquine (PQ) and sitamaquine (Sit) with their  $pK_a$  values which weakly fits a power correlation. This weak correlation partly reflects the separate mechanistic origin of their  $pK_a$  values. Thus although protonation of 5-A-6-MeQ and 2-AQ-3-CN involves the substituent  $\text{NH}_2$  group, protonation of Q is on the heterocyclic

**Table 2**

Number and length of H-bonds formed from and binding energies of, most probable (MP) and lowest energy (LE) conformer of AQ and *s*-AQ with polar groups of phospholipid bilayers.

Compound	H-bonds /number, length/nm	Binding energy (MP)/ Kcal/mol	Binding energy (LE)/ Kcal/mol
Q	0	-6.18	-6.3
2-AQ	2 0.25, 0.21	-5.92	-6.07
3-AQ	1 0.2	-6.16	-6.16
4-AQ	1 0.21	-6.25	-6.25
5-AQ	1 0.21	-6.26	-6.26
6-AQ	2 0.23,0.25	-6.03	-6.07
7-AQ	0	-6.22	-6.22
8-AQ	1 0.23	-5.3	-6.06
5-A-6-MeQ	0	-5.9	-6.73
2-AQ-3-CN	0	-6.1	-6.18
PQ	0	-5.1	-6.13
Sit	0	-5.4	-7.17

N. Both PQ and Sit are protonated on their side chain amine group which dissociates at the solution pH values corresponding to their respective  $pK_a$  values. Their higher  $pK_a$  values (Table 1) shows that the PQ and Sit are charged at  $\sim 100\%$  protonation in pH 7.4 solution and this will be one of the main factors promoting the PQ and Sit interaction with the

phospholipid layers. The literature on Sit [59,60] and PQ [6] interaction with both model and *in vitro* cell phospholipid membranes is quite extensive. The general conclusion is that the positively charged quarternary nitrogen on the side chain is responsible for the initial interaction with the polar groups' negatively charged phosphate. This is followed by the insertion of the Q rings within the apolar alkyl chain core of the lipid membrane [6,59,60]. From the evidence in this study, it also appears that the alkyl chain with positively charged quarternary nitrogen instigates the interaction followed by the insertion of the Q rings. The electron withdrawing feature of the alkyl chain attached to quarternary ammonium group with positive Hammetts constant [63] will lower the electron density in the Q ring lessening its interaction with the phospholipid layer. However, a factor promoting the interaction of PQ and Sit with the phospholipid layer is the length of the alkyl chain containing the quarternary nitrogen group. The estimated value for  $\log D$  assumes that in terms of thermodynamic partition into the phospholipid layer, only the neutral molecule partitions into the layer. However this is not the case since it is known that charged organic molecules can interact strongly with lipid layers as discussed above. In addition the apolarity of the alkyl chain can greatly assist the initial interaction. This is most certainly the case in this instance since the 'log BAI' value is 2.2 for PQ and 1.15 for Sit/phospholipid interaction. On the other hand the 'log BAI' value is  $< 1$  for 4-AQ/phospholipid interaction and 4-AQ is similarly charged to PQ and Sit in aqueous solution at pH 7.4.

One interesting anomaly is that it has been observed that when positively charged inorganic [52] and organic [4] ions adsorb on the DOPC layer, the subsequent interaction causes both capacitance current peaks to shift to a more positive potential in accordance with the Esin-

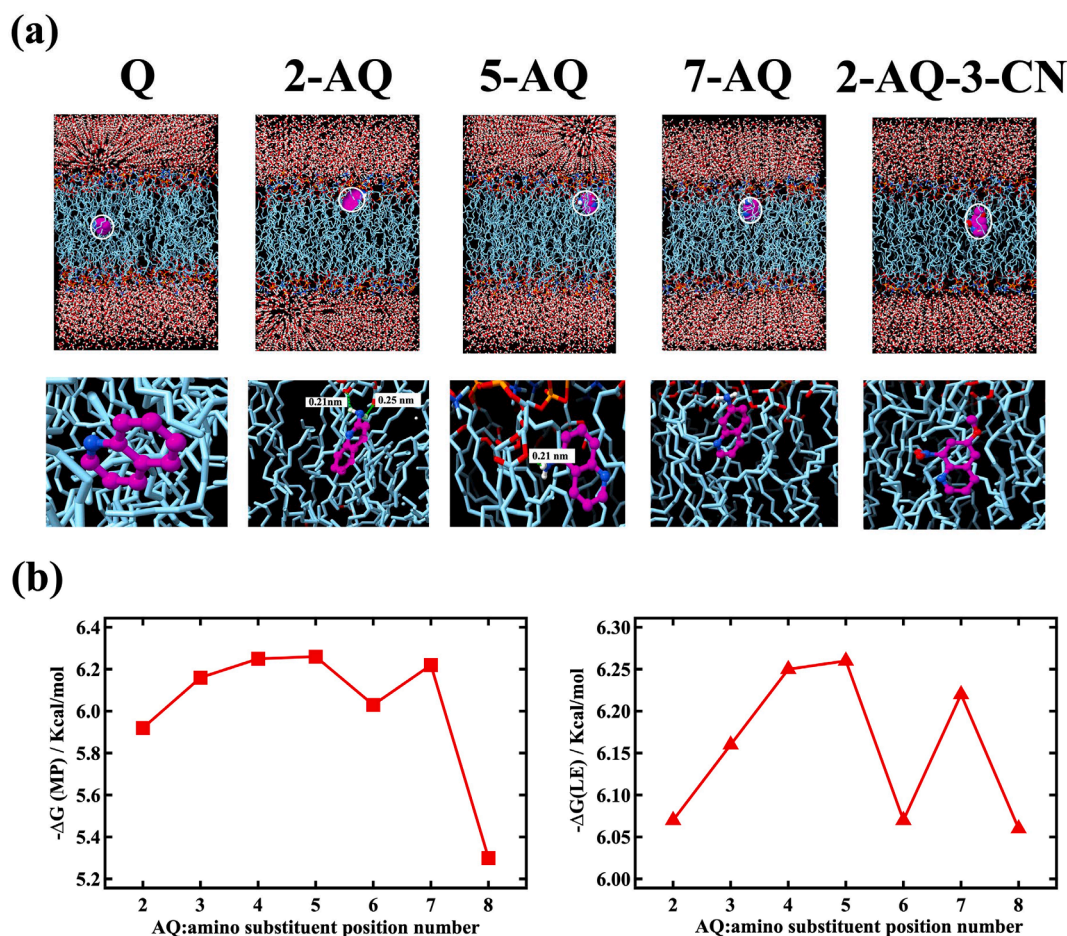


**Fig. 7.** (a) (top) most probable (MP) position (white encircled) of representative AQ and *s*-AQs in apolar region (blue) of phospholipid bilayer and (bottom) relation to polar groups with lengths for AQ-DOPC H-bonds and, (b) binding energies (left MP and right LE) for AQs vs amino substituent position number from Table 2.

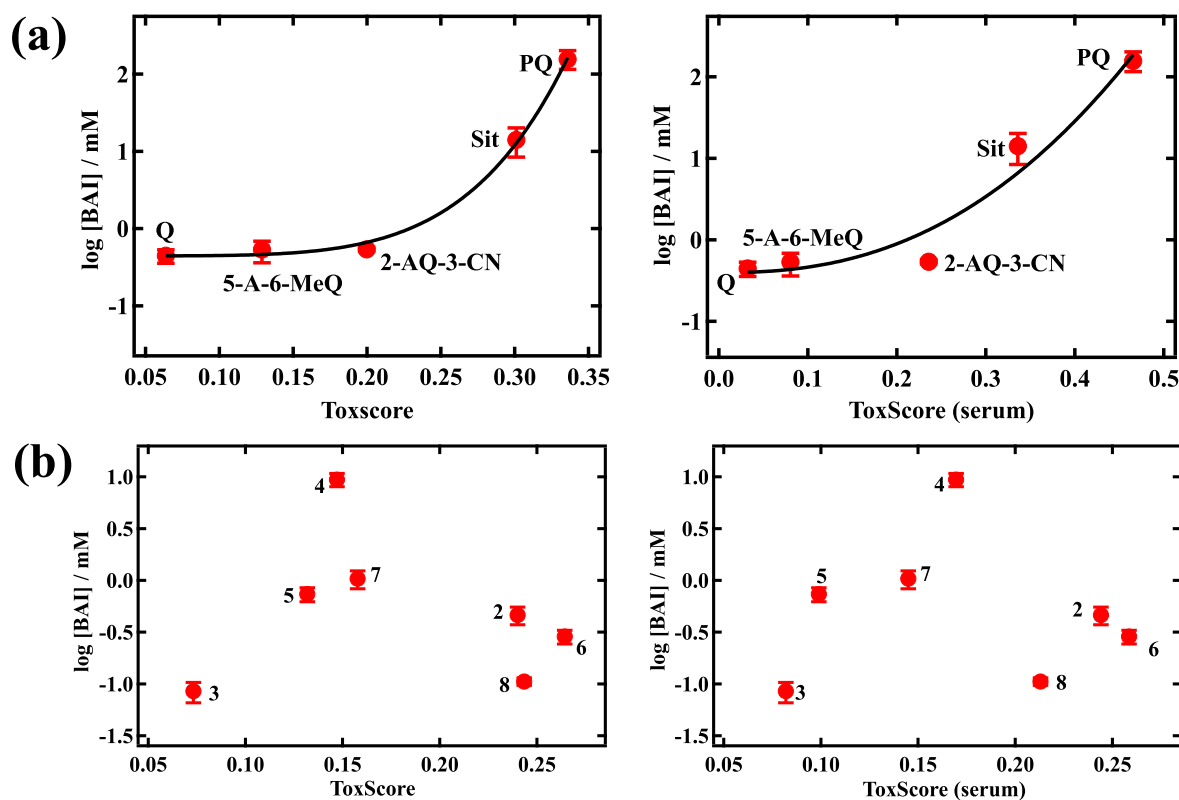


Fig. 8. (a) *s*-AQ and (b) AQ 'log BAI' vs ToxScore and ToxScore (serum) plot.

Markov effect [52,64]. In the present studies, although it is known that 4-AQ, PQ and Sit are present as protonated ions in pH 7.4 solution, only the 4-AQ/DOPC interaction gives rise to a significant positive potential shift of capacitance peak current peaks. Since this is also observed as a result of 2- and 3-AQ interaction which are protonated to lesser and negligible extent respectively, it cannot be conclusively deduced that this potential shift of capacitance peak current is caused by positive charged ions adsorbed within the phospholipid layer.

The modelling results of the AQ interaction with DOPC phospholipid bilayer showed the following features displayed in Table 2, Fig. 7(a) and 7(b) and Fig. S5 in the SI.

2-,3-,4-,5-, 6- and 8-AQ exhibited H-bonding however 7-AQ showed no H-bond with the phospholipid polar groups and a deeper position in the bilayer. As a control Q showed no H-bonding with the polar groups and a deeper position compared to that of 7-AQ in the bilayer. 5-A-6-MeQ and 2-AQ-3-CN showed no H-bonding and similarly a deep position in the bilayer (see Fig. 7(a) and Fig. S5 in the SI). It seems that the marked positive potential shifts of the capacity current peaks on the RCV resulting from 2-, 3- and 4-AQ/DOPC interaction (Fig. 2(a) and Fig. S2 in the SI) are related to the H-bonding of the AQ amino group with the polar groups as exhibited in the modelling results (Table 2, Fig. 7(a) and Fig. S5 in the SI) and the association of the cationic 4-AQ with the anionic phosphate grouping. In addition the 5-A-6-MeQ interaction with DOPC exhibits no capacitance peak shift on the RCV. This indicates that its most probable conformation is dominated by the modelling results showing a deeper position in the phospholipid layer and no H-bonding with the DOPC polar groups. The influence of organic compound charge on their depth in the phospholipid layer following interaction is of great interest and has been extensively modelled [65]. Using this argument, the relatively small capacity current peak shifts following interaction of PQ and Sit with the layer show that, even though these molecules are 100 % positively charged, on interaction they are drawn deeper into the DOPC layer effected by their longer alkyl side chain. To summarise, these results show that the AQ and *s*-AQ location in the bilayer is

determined by opposing directional forces of the propensity for the  $-NH_2$  group to H-bond with the bilayer surface polar groups and the non-covalent associations between the quinoline rings/polarisable substituents and the phospholipid alkyl chains.

An exception to the argument connecting capacitance current peak shift to occurrence of significant H-bonding of the AQ with the polar groups of the DOPC is 8-AQ/DOPC interaction and is explained in the following. Significantly with 8-AQ the H-bonding potential of the  $NH_2$  group is weakened compared to that of 3-AQ due to intramolecular H-bonding with the nuclear N atom [66] leading to zero shifts in the RCV capacity current peak potential. This effect is currently being investigated. Significantly, two outliers in the 'log BAI' versus  $pK_a$  plot for the AQs can be related to the H-bonding potential of the AQs. Both 2- and 3-AQ fall below the linear plot and it can be assumed the H-bonding decreases the ability of the Q rings to interact with the lipid alkyl chains.

A plot of AQ binding energies versus  $-NH_2$  position (see Fig. 7(b)) exhibit the two peaked plot where the 5- and 7-AQ binding energies peak similarly to the  $-\log LoD$  versus  $-NH_2$  position plot. The higher binding energy (Table 2) and deeper position (Fig. 8 and Fig. S5 in the SI) of 5-AQ in the bilayer can explain its higher  $-LoD$  and 'log BAI' value which accounts for its being an outlier in the 'log BAI' versus  $pK_a$  plot. It is noted that the 2- and 4-AQ binding energies are lower than expected. This could be because the AUTODOCK program does not account for cationic molecular interaction since 2- and 4-AQ molecules are  $\sim 50\%$  and  $\sim 100\%$  respectively charged at pH 7.4. Due to the fact that both PQ and Sit are charged molecules and that PQ has a 7-carbon side chain which can present problems with the AUTODOCK application [67], an analysis into the *s*-AQ binding energies with bilayers and their relation with the experimental data will be investigated in future studies.

Fig. 8 shows correlations between the 'log BAI' and the ToxScore for (a) the *s*-AQ compounds. The correlation between 'log BAI' and the ToxScore with and without serum is good and fits a power function. It can be surmised that the compound's 'log BAI' value is related, in a very general way, to the interaction of the compound with biological

material. In this case the positive charge on the *s*-AQ is the most significant descriptor above the lipophilicity enhancing interaction with phospholipid layers and the *in vitro* biological targets. The relationship between the AQ 'log BAI' and the AQ ToxScore (Fig. 8(b)) is not so straightforward and could be complicated by the extensive H-bonding of some AQs with the phospholipid polar groups shown in the modelling and, experimentally inferred from the RCV shape. A linear relationship is seen for 3-, 4-, 5- and 7-AQ but no relationship is observed for 2-, 6- and 8-AQ which have a low 'log BAI' and a higher ToxScore value. A possible explanation is that these molecules exhibit a high degree of H-bonding with the phospholipid polar groups which accounts for a stronger interaction with biological material but weaker 'log BAI' index. The ToxScore of 3-AQ is low and is an exception to this concept. Clearly more experiments would need to be carried out to explore this.

#### 4. Conclusion

AQ and *s*-AQ interact with phospholipid layers. The electrochemical (bio)membrane sensor records adsorption and partition of the compound on and into the layer respectively as well as aspects of the specific interaction relating to H-bonding and non-covalent interactions. HPLC-IAM technology measures the partition coefficient between the solution and phospholipid layer including partition due to interaction of the positive molecular charge with the anionic phosphate of the phospholipid polar heads. The affinity above the lipophilicity of AQ with the phospholipid layer shows a linear relationship with the compound's  $pK_a$  which is linked directly to the molecular charge and to the increased polarisability of the AQ's aromatic rings. Outliers in this correlation can be due to the presence/absence of H-bonding between the AQ and the polar groups and a more superficial/deeper location in the layer. The association of the unsubstituted AQs with the phospholipid layer represents an interplay between the molecules' propensity to bind to the phospholipid polar groups and the strength of the non-covalent interaction between the AQ's Q rings and the apolar region of the layer. *s*-AQ interactions with the phospholipid layer exhibit an affinity above their lipophilicity which shows a power relationship with a ToxScore value of the compound derived from five different *in vitro* end points. In this case the *s*-AQ descriptor of positive molecular charge which enhances interaction with phospholipid layers presumably leads to the binding of these compounds to the *in vitro* biological targets.

#### CRedit authorship contribution statement

**Bethany Crow:** Writing – original draft, Methodology, Investigation, Conceptualization. **Roland Grafstrom:** Methodology. **Vesa Hongisto:** Methodology, Investigation, Formal analysis, Data curation. **Mitali Kamat:** Software, Methodology. **Nikil Kapur:** Supervision, Project administration, Methodology. **Ross Kelly:** Resources, Conceptualization. **Josh Owen:** Supervision, Methodology. **Ashi Rashid:** Visualization, Validation, Software, Methodology, Investigation. **William Stokes:** Supervision, Methodology. **Nicola William:** Methodology, Investigation, Conceptualization. **Jeanine Williams:** Methodology, Investigation, Formal analysis, Data curation. **Andrew Nelson:** Writing – original draft.

#### Declaration of competing interest

The authors declare that they have no known competing financial interests or personal relationships that could have appeared to influence the work reported in this paper.

#### Acknowledgements

This work was funded through the EU Horizon 2020 Programmes: HISENTS and SABYDOMA, Grant agreement Nos: 685817 and 862296 respectively and through the UKRI Horizon Europe Guarantee fund Bio-

SUSHY Grant reference No: 10056199. Thanks to Dr Klara Valko, Bio-Mimetic Chromatography Ltd, for helpful advice on the use of IAM technology.

#### Appendix A. Supplementary data

Supplementary data to this article can be found online at <https://doi.org/10.1016/j.bioelechem.2025.108927>.

#### Appendix C. Supplementary data

Supplementary data to this article can be found online at <https://doi.org/10.1016/j.bioelechem.2025.108927>.

#### Data availability

Data will be made available on request.

#### References

- [1] C. Hansch, Quantitative approach to biochemical structure-activity relationships, *Acc. Chem. Res.* 2 (1969) 232–239, <https://doi.org/10.1021/ar50020a002>.
- [2] R. Guha, On exploring structure–activity relationships, *In Silico Models for Drug Discovery* (2013) 81–94, [https://doi.org/10.1007/978-1-62703-342-8\\_6](https://doi.org/10.1007/978-1-62703-342-8_6).
- [3] J.J. Sutherland, L.A. O'Brien, D.F. Weaver, A comparison of methods for modeling quantitative structure–activity relationships, *J. Med. Chem.* 47 (2004) 5541–5554, <https://doi.org/10.1021/jm049714>.
- [4] N. William, A. Nelson, S. Gutsell, G. Hodges, J. Rabone, A. Teixeira, Hg-supported phospholipid monolayer as rapid screening device for low molecular weight narcotic compounds in water, *Anal. Chim. Acta* 1069 (2019) 98–107, <https://doi.org/10.1016/j.aca.2019.04.019>.
- [5] S. Mohamadi, D.J. Tate, A. Vakurov, A. Nelson, Electrochemical screening of biomembrane-active compounds in water, *Anal. Chim. Acta* 813 (2014) 83–89, <https://doi.org/10.1016/j.aca.2014.01.009>.
- [6] L.G. Basso, R.Z. Rodrigues, R.M. Naal, A.J. Costa-Filho, Effects of the antimalarial drug primaquine on the dynamic structure of lipid model membranes, *Biochimica et Biophysica Acta (BBA)-Biomembranes* (1808 (2011)) 55–64, <https://doi.org/10.1016/j.bbamem.2010.08.009>.
- [7] P.L. Olliaro, P. Mussano, *Cochrane Infectious Diseases Group, Amodiaquine for treating malaria*, *Cochrane Database Syst. Rev.* 2019 (1996), <https://doi.org/10.1002/14651858.CD000016>.
- [8] T.E. Wellems, C.V. Plowe, Chloroquine-resistant malaria, *J Infect Dis* 184 (2001) 770–776, <https://doi.org/10.1086/322858>.
- [9] World Health Organization. World Health Organization Model List of Essential Medicines, 21st List, 2021 ed. Geneva: World Health Organization, 201 [Accessed from 22nd April 2021]. Available from: <https://www.who.int/publications/i/item/WHOMVPMPPIAU2019.06>.
- [10] M.A. Shibeshi, Z.D. Kifle, S.A. Atmafie, Antimalarial drug resistance and novel targets for antimalarial drug discovery, *Infect. Drug Resist.* 13 (2020) 4047–4060, <https://doi.org/10.2147/IDR.S279433>.
- [11] Q. Huynh Hong, K. Chau Van, H. Phạm Thanh, N. Nguyen Thanh Thuy, N. Do Van, S. Tran Thanh, H. Huynh Nguyen Ngan, D. Ly Thai, H. Nguyen Duc, Serious antimalaria resistance, genetic markers of Kelch 13, plasmepsine 2 CNV associated with dihydroartemisinin-piperazine phosphate resistance in Plasmodium falciparum population in malaria hyperendemic zone of Dak Lak Province (2019–2020). *World Journal of Advanced Research and Reviews* 8 (2020) 246–253. DOI: 10.30574/wjarr.2020.8.1.0395.
- [12] M. Dagen, History of malaria and its treatment. In: Patrick, G.L. ed. *Antimalarial Agents: Design and Mechanism of Action*. Elsevier, 2020, pp. 1–48. DOI: 10.1016/B978-0-08-101210-9.00001-9.
- [13] P.M. Loiseau, S. Cojean, J. Schrével, Sitamaquine as a putative antileishmanial drug candidate: from the mechanism of action to the risk of drug resistance, *Parasite: Journal De La Société Française De Parasitologie* 18 (2011) 115, <https://doi.org/10.1051/parasite/2011182115>.
- [14] X. Liu, B. Testa, A. Fahr, Lipophilicity and its relationship with passive drug permeation, *Pharmaceutical Research* 28 (2011) 962–977, <https://doi.org/10.1007/s11095-010-0303-7>.
- [15] N. Timmer, S.T. Droge, Sorption of cationic surfactants to artificial cell membranes: comparing phospholipid bilayers with monolayer coatings and molecular simulations, *Environ. Sci. Tech.* 51 (2017) 2890–2898, <https://doi.org/10.1021/acs.est.6b05662>.
- [16] D. Bemporad, C. Luttmann, J.W. Essex, Behaviour of small solutes and large drugs in a lipid bilayer from computer simulations, *Biochimica et Biophysica Acta (BBA)-Biomembranes* (1718 (2005)) 1–21, <https://doi.org/10.1016/j.bbamem.2005.07.009>.
- [17] V.S. Inakollu, D.P. Geerke, C.N. Rowley, H. Yu, Polarizable force fields: what do they add in biomolecular simulations? *Curr. Opin. Struct. Biol.* 61 (2020) 182–190, <https://doi.org/10.1016/j.sbi.2019.12.012>.

- [18] L. Xing, R.C. Glen, Novel methods for the prediction of log *P*, p*K*<sub>a</sub> and log *D*, *J. Chem. Inf. Comput. Sci.* 42 (2002) 796–805, <https://doi.org/10.1021/ci010315d>.
- [19] D.H. McDaniel, H.C. Brown, An extended table of Hammett substituent constants based on the ionization of substituted benzoic acids, *J. Org. Chem.* 23 (1958) 420–427, <https://doi.org/10.1021/jo01097a026>.
- [20] I. Aliagas, A. Gobbi, M.L. Lee, B.D. Sellers, Comparison of log *P* and log *D* correction models trained with public and proprietary data sets, *J. Comput. Aided Mol. Des.* 36 (2022) 253–262, <https://doi.org/10.1007/s10822-022-00450-9>.
- [21] A. Albert R. Goldacre J.N. Phillips T. Strength of Heterocyclic Bases, *J. Chem. Soc.* 2240-9 DOI 1948 10.1039/JR9480002240.
- [22] Comp Tox Chemicals Dashboard v2 4.0, US Environmental Protection, Agency (2024), K. Mansouri, C.M. Grulke, R.S Judson, A.J. Williams, OPERA models for predicting physicochemical properties and environmental fate endpoints, *Journal of Cheminformatics* 10 (2018) 1-19. DOI: 10.1186/s13321-018-0263-1. A.J. Williams, C.M. Grulke, J. Edwards, A.D. McEachran, K. Mansouri, N.C. Baker, G. Patlewicz, I. Shah, J.F. Wambaugh, R.S. Judson, A.M. Richard, The CompTox Chemistry Dashboard: a community data resource for environmental chemistry. *Journal of Cheminformatics* 9 (2017) 1-27. DOI: 10.1186/s13321-017-0247-6.
- [23] S. Ong, H.H. Liu, C. Pidgeon, Immobilized-artificial-membrane chromatography: measurements of membrane partition coefficient and predicting drug membrane permeability, *J. Chromatogr. A* 728 (1996) 113–128, [https://doi.org/10.1016/0021-9673\(95\)00837-3](https://doi.org/10.1016/0021-9673(95)00837-3).
- [24] T Abdelilah, C. Oussama, A. El Aissouq, E.O. Youssef, M. Bouachrine, A. Ouammou, A., Prediction of Novel TRPV1 Antagonist: A Combination of 3D-QSAR, Molecular Docking, MD Simulations and ADMET Prediction. *Physical Chemistry Research* 11 (2023) 353-368. DOI: 10.22036/PCR.2022.334832.2059.
- [25] B. Bicak, S.K. Gündüz, Y. Kökcü, A.E. Özel, S. Akyüz, Molecular docking and molecular dynamics studies of L-glycyl-L-glutamic acid dipeptide, *Bilge International Journal of Science and Technology Research* 3 (2019) 1–9, <https://doi.org/10.30516/bilgesci.476841>.
- [26] A. El Aissouq, O. Chedadi, R. Kasmi, L. Elmchichi, F. En-nahli, A. Goudzal, M. Bouachrine, A. Ouammou, F. Khalil, Molecular modeling studies of C-Glycosylflavone derivatives as GSK-3β inhibitors based on QSAR and docking analysis, *J. Solution Chem.* 50 (2021) 808–822, <https://doi.org/10.1007/s10953-021-01083-6>.
- [27] M. Matossian, C. Vangelder, P. Papagerakis, L. Zheng, G.T. Wolf, S. Papagerakis, S., In silico modeling of the molecular interactions of anticancer medication with the endothelium: novel therapeutic implications in head and neck carcinomas, *International Journal of Immunopathology and Pharmacology* 27(2014) 573-583. DOI: 10.1177/039463201402700413.
- [28] A.R. Collins, B. Annangi, L. Rubio, R. Marcos, M. Dorn, C. Merker, I. Estrela-Lopis, M.R. Cimpan, M. Ibrahim, E. Cimpan, M. Ostermann, High throughput toxicity screening and intracellular detection of nanomaterials, *Wiley Interdisciplinary Reviews: Nanomedicine and Nanobiotechnology* 9 (2017) e1413.
- [29] Y. Kohl, N. William, E. Elje, N. Backes, M. Rothbauer, A. Srancikova, E. Runden-Pran, N. El Yamani, R. Korenstein, L. Madi, A. Barbul, K. Kozics, M. Sramkova, K. Steenson, A. Gabelova, P. Ertl, M. Dusinska, A. Nelson, Rapid identification of in vitro cell toxicity using an electrochemical membrane screening platform, *Bioelectrochemistry* 153 (2023) 108467, <https://doi.org/10.1016/j.bioelechem.2023.108467>.
- [30] J. Owen, M. Kuznecovs, R. Bhamji, N. William, N. Domenech-Garcia, M. Hesler, T. Knoll, Y. Kohl, A. Nelson, N. Kapur, High-throughput electrochemical sensing platform for screening nanomaterial–biomembrane interactions, *Rev Sci Instrum* 91 (2020) 025002, <https://doi.org/10.1063/1.5131562>.
- [31] Z. Coldrick, A. Penezić, B. Gašparović, P. Steenson, J. Merrifield, A. Nelson, High throughput systems for screening biomembrane interactions on fabricated mercury film electrodes, *J Appl Electrochem* 41 (2011) 939–949, <https://doi.org/10.1007/s10800-011-0319-7>.
- [32] R. Pawliczak, M.J. Cowan, X. Huang, U.B. Nanavaty, S. Alsaaty, C. Logun, J. H. Shelhamer, p11 expression in human bronchial epithelial cells is increased by nitric oxide in a cGMP-dependent pathway involving protein kinase G activation, *J. Biol. Chem.* 276 (2001) 44613–44621, <https://doi.org/10.1074/jbc.M104993200>.
- [33] Y.L. Zhao, C.Q. Piao, L.J. Wu, M. Suzuki, T.K. Hei, Differentially expressed genes in asbestos-induced tumorigenic human bronchial epithelial cells: implication for mechanism, *Carcinogenesis* 21 (2000) 2005–2010, <https://doi.org/10.1093/carcin/21.11.2005>.
- [34] X. Liu, T. Umino, M. Cano, R. Ertl, T. Veys, J. Spurzem, D. Romberger, S.I. Rennard, Human bronchial epithelial cells can contract type I collagen gels, *American Journal of Physiology-Lung Cellular and Molecular Physiology* 274 (1998) L58–L65, <https://doi.org/10.1152/ajplung.1998.274.1.L58>.
- [35] T.K. Hei, L.J. Wu, C.Q. Piao, Malignant transformation of immortalized human bronchial epithelial cells by asbestos fibers, *Environ. Health Perspect.* 105 (1997) 1085–1088, <https://doi.org/10.1289/ehp.9710551085>.
- [36] J.F. Lechner, M.A. LaVeck, A serum-free method for culturing normal human bronchial epithelial cells at clonal density, *J. Tissue Cult. Methods* 9 (1985) 43–48, <https://doi.org/10.1007/BF01797773>.
- [37] I.R. Miller, J. Rishpon, A. Tenenbaum, Electrochemical determination of structure and interactions in spread lipid monolayers, *Bioelectrochem Bioenerg* 3 (1976) 528–542, [https://doi.org/10.1016/0302-4598\(76\)80043-8](https://doi.org/10.1016/0302-4598(76)80043-8).
- [38] A. Nelson, A. Benton, Phospholipid monolayers at the mercury/water interface, *J. Electroanal. Chem. Interfacial Electrochem.* 202 (1986) 253–270, [https://doi.org/10.1016/0022-0728\(86\)90123-3](https://doi.org/10.1016/0022-0728(86)90123-3).
- [39] A. Nelson, Electrochemistry of mercury supported phospholipid monolayers and bilayers, *Curr. Opin. Colloid Interface Sci.* 15 (2010) 455–466, <https://doi.org/10.1016/j.cocis.2010.07.004>.
- [40] A. Nelson, Conducting gramicidin channel activity in phospholipid monolayers, *Biophys. J.* 80 (2001) 2694–2703, [https://doi.org/10.1016/S0006-3495\(01\)76238-8](https://doi.org/10.1016/S0006-3495(01)76238-8).
- [41] M.R. Moncelli, L. Becucci, A. Nelson, R. Guidelli, Electrochemical modeling of electron and proton transfer to ubiquinone-10 in a self-assembled phospholipid monolayer, *Biophys. J.* 70 (1996) 2716–2726, [https://doi.org/10.1016/S0006-3495\(96\)79841-7](https://doi.org/10.1016/S0006-3495(96)79841-7).
- [42] A. Nelson, F.A.M. Leermakers, Substrate-induced structural changes in electrode-adsorbed lipid layers: experimental evidence from the behaviour of phospholipid layers on the mercury-water interface, *J. Electroanal. Chem. Interfacial Electrochem.* 278 (1990) 73–83, [https://doi.org/10.1016/0022-0728\(90\)85124-N](https://doi.org/10.1016/0022-0728(90)85124-N).
- [43] A.V. Brukhno, A. Akinshina, Z. Coldrick, A. Nelson, S. Auer, Phase phenomena in supported lipid films under varying electric potential, *Soft Matter* 7 (2011) 1006–1017, <https://doi.org/10.1039/c0sm00724b>.
- [44] A. Vakurov, M. Galluzzi, A. Podesta, N. Gamper, A.L. Nelson, S.D. Connell, Direct characterization of fluid lipid assemblies on mercury in electric fields, *ACS Nano* 8 (2014) 3242–3250, <https://doi.org/10.1021/NN4037267>.
- [45] N. Ormatégui, S. Zhang, I. Loiaz, R. Brydson, A. Nelson, A. Vakurov, Interaction of poly (N-isopropylacrylamide)(pNIPAM) based nanoparticles and their linear polymer precursor with phospholipid membrane models, *Bioelectrochemistry* 87 (2012) 211–219, <https://doi.org/10.1016/j.bioel.2011.12.006>.
- [46] A. Vakurov, R. Brydson, A. Nelson, Electrochemical modelling of the silica nanoparticle–biomembrane interaction, *Langmuir* 28 (2012) 1246–1255, <https://doi.org/10.1021/LA203568N>.
- [47] Z. Coldrick, P. Steenson, P. Millner, M. Davies, A. Nelson, Phospholipid monolayer coated microfabricated electrodes to model the interaction of molecules with biomembranes, *Electrochim Acta* 54 (2009) 4954–4962, <https://doi.org/10.1016/j.jelectacta.2009.02.095>.
- [48] D. Chapman, Phase transitions and fluidity characteristics of lipids and cell membranes, *Q. Rev. Biophys.* 8 (1975) 185–235, <https://doi.org/10.1017/S0033583500001797>.
- [49] I. Zawisza, X. Bin, J. Lipkowski, Spectroelectrochemical studies of bilayers of phospholipids in gel and liquid state on Au (111) electrode surface, *Bioelectrochemistry* 63 (2004) 137–147, <https://doi.org/10.1016/j.bioelechem.2003.12.004>.
- [50] G. Valincius, T. Meskauskas, F. Ivanauskas, Electrochemical impedance spectroscopy of tethered bilayer membranes, *Langmuir* 28 (2012) 977–990, <https://doi.org/10.1021/la204054g>.
- [51] R. Budvytyte, G. Valincius, G. Niaura, V. Voiciuk, M. Mickevicius, H. Chapman, H. Z. Goh, P. Shekhar, F. Heinrich, S. Shenoy, M. Lösche, Structure and properties of tethered bilayer lipid membranes with unsaturated anchor molecules, *Langmuir* 29 (2013) 8645–8656, <https://doi.org/10.1021/la401132c>.
- [52] A. Rashid, A. Vakurov, A. Nelson, Role of electrolyte in the occurrence of the voltage induced phase transitions in a dioleoyl phosphatidylcholine monolayer on Hg, *Electrochim Acta* 155 (2015) 458–465, <https://doi.org/10.1016/j.electacta.2014.12.077>.
- [53] L. Becucci, S. Martinuzzi, E. Monetti, R. Mercatelli, F. Quercioli, D. Battistel, R. Guidelli, Electrochemical impedance spectroscopy and fluorescence lifetime imaging of lipid mixtures self-assembled on mercury, *Soft Matter* 6 (2010) 2733–2741, <https://doi.org/10.1039/b923895f>.
- [54] L. Becucci, R. Guidelli, F. Polo, F. Maran, Interaction of mixed-ligand monolayer-protected Au144 clusters with biomimetic membranes as a function of the transmembrane potential, *Langmuir* 30 (2014) 8141–8151, <https://doi.org/10.1021/la500909j>.
- [55] X. Wang, S. Ma, Y. Su, Y. Zhang, H. Bi, L. Zhang, X. Han, High impedance droplet–solid interface lipid bilayer membranes, *Anal. Chem.* 87 (2015) 2094–2099, <https://doi.org/10.1021/AC502953V>.
- [56] P.S. Ghosal, A.K. Gupta, Determination of thermodynamic parameters from Langmuir isotherm constant-revisited, *J. Mo.I. Liq.* 225 (2016) 137–146. DOI: 10.1016/j.molliq.2016.11.058.
- [57] S.T.J. Droge, J.L.M. Hermens, J. Rabone, S. Gutsell, G. Hodges, Phospholipophilicity of C<sub>x</sub>H<sub>y</sub>N<sup>+</sup> amines: chromatographic descriptors and molecular simulations for understanding partitioning into membranes, *Environ. Sci. Processes Impacts* 18 (2017) 1011–1023, <https://doi.org/10.1039/C6EM00118A>.
- [58] A. Albert, R. Goldacre, Basicities of the aminoquinolines: comparison with the aminoacridines and aminopyridines, *Nature* 153 (1944) 467–469, <https://doi.org/10.1038/153467b0>.
- [59] A.M. Dueñas-Romero, P.M. Loiseau, M. Saint-Pierre-Chazalet, Interaction of sitamaquine with membrane lipids of *Leishmania donovani* promastigotes, *Biochimica et Biophysica Acta (BBA)-Biomembranes* 1768 (2007) 246–252, <https://doi.org/10.1016/j.bbamem.2006.07.003>.
- [60] P.M. Loiseau, S. Cojean, J. Schrével, Sitamaquine as a putative antileishmanial drug candidate: from the mechanism of action to the risk of drug resistance. *Parasite: journal de la Société Française de Parasitologie* 18(2011) 115. DOI: 10.1051/parasite/2011182115.
- [61] D. Vrakas, C. Giaginis, A. Tsantili-Kakoulidou, Electrostatic interactions and ionization effect in immobilized artificial membrane retention: a comparative study with octanol–water partitioning, *J. Chromatogr. A* 1187 (2008) 67–78, <https://doi.org/10.1016/j.chroma.2008.01.079>.
- [62] G.B. Barlin, D.D. Perrin, Prediction of the strengths of organic acids, *Q. Rev. Chem. Soc.* 20 (1966) 75–101, <https://doi.org/10.1039/QR9662000075>.

- [63] C. Hansch, A. Leo, R.W. Taft, A survey of Hammett substituent constants and resonance and field parameters, *Chem. Rev.* 91 (1991) 165–195, <https://doi.org/10.1021/cr00002a004>.
- [64] A. Frumkin, O. Petry, A. Kossaya, V. Entina, V. Topolev, Electric double layer on platinum-group metals and the Esin-Markov effect, *J. Electroanal. Chem. Interfacial Electrochem.* 16 (1968) 175–191, [https://doi.org/10.1016/S0022-0728\(68\)80060-9](https://doi.org/10.1016/S0022-0728(68)80060-9).
- [65] K. Bittermann, S. Spycher, K.U. Goss, Comparison of different models predicting the phospholipid-membrane water partition coefficients of charged compounds, *Chemosphere* 144 (2016) 382–391, <https://doi.org/10.1016/j.chemosphere.2015.08.065>.
- [66] N. Leroux, M. Goethals, T. Zeegers-Huyskens, Infrared study of the hydrogen bonding ability of 3-aminoquinoline and 8-aminoquinoline, *Vib. Spectrosc.* 9 (1995) 235–243, [https://doi.org/10.1016/0924-2031\(95\)00019-Q](https://doi.org/10.1016/0924-2031(95)00019-Q).
- [67] A. Dhanik, J.S. McMurray and Kavradi, 2012, October. Autodock-based incremental docking protocol to improve docking of large ligands. In *2012 IEEE International Conference on Bioinformatics and Biomedicine Workshops* pp. 48-55, IEEE.